Journal of Applied Polymer Science

Evolution of the Properties of a Poly(L-lactic acid) Scaffold with Double Porosity During *In Vitro* Degradation in a Phosphate-Buffered Saline Solution

Harmony Deplaine,[1] Victor A. Acosta-Santamaría,[2,3] Ana Vidaurre,[1,4] José Luis Gómez Ribelles,[1,4] Manuel Doblaré,[2,4] Ignacio Ochoa,[2,4] Gloria Gallego Ferrer[1,4]

[1]Center for Biomaterials and Tissue Engineering, Universitat Politècnica de València, 46022 Valencia, Spain

[2]Group of Structural Mechanics and Materials Modelling, Aragón Institute of Engineering Research, University of Zaragoza, 50009 Zaragoza, Spain

[3]Aragon Institute of Technology, 50009 Zaragoza, Spain

[4]Biomedical Research Networking Center in Bioengineering, Biomaterials, and Nanomedicine, 50018 Zaragoza, Spain

Correspondence to: A. Vidaurre (E-mail: vidaurre@fis.upv.es)

ABSTRACT: A poly(L-lactic acid) scaffold prepared by a combination of freeze-extraction and porogen-leaching methods was submitted to static degradation in a phosphate-buffered saline solution at pH 7.4 and 37°C for up to 12 months. After 6 months of degradation, the scaffold maintained its integrity, although noticeable changes in its permeability and pore size were recorded. After 12 months, scanning electron microscopy pictures showed that most of the trabeculae were broken, and the sample disaggregated under minimum loading. Neither weight loss nor crystallinity changes in the first heating calorimetric scan were observed during the degradation experiment. However, after 12 months, a rise in the crystallinity from 13 to 38% and a drop in the glass-transition temperature from 58 to 54°C were measured in the second heating scan. The onset of thermal degradation moved from 300 to 210°C after 12 months. Although the elastic modulus suffered only a very slight reduction with degradation time, the aggregate modulus decreased 44% after 6 months. © 2014 Wiley Periodicals, Inc. J. Appl. Polym. Sci. **2014**, *131*, 40956.

KEYWORDS: biomedical applications; degradation; mechanical properties

Received 3 March 2014; accepted 2 May 2014

DOI: 10.1002/app.40956

INTRODUCTION

Tissue engineering, which is based on cell transplantation in combination with supportive porous scaffolds and biomolecules, is mainly focused on restoring the structure of tissues damaged by illness or traumatism. The porous scaffold serves as a three-dimensional template for initial cell attachment and subsequent tissue formation. The scaffold gradually degrades while the new tissue develops. It is well known that the scaffold architecture and mechanical properties have decisive effects on the regenerating tissue.[1] Changes in the scaffold properties during degradation are of crucial importance in the long-term success of a tissue-engineered cell–polymer construct. The rate of degradation may affect many cellular processes, including cell growth, tissue regeneration, and host response.

Biodegradable scaffolds intended for tissue engineering must meet different requirements,[2] including a high porosity, adequate pore size, and interconnected pore network, and they must have suitable mechanical properties. The scaffold should maintain the integrity of the designed structure and provide sufficient temporary mechanical support to withstand loading on the site of the implant.[3,4] The stress–strain response of the scaffold should be similar to that of the tissue surrounding the injured area to deliver the appropriate mechanical signals to the cells to promote proper extracellular matrix production. Furthermore, as has been recently emphasized, the scaffold should remain at the site of injury until tissue formation, remodeling, and maturation occur.[5]

Scaffold pore configuration, that is, pore size, porosity, and interconnectivity, is of special importance in scaffold design.[6,7] Its permeability, which is closely related to its pore interconnectivity, is also an important parameter, as it helps to control cell migration into the scaffold and diffusion of nutrients and waste products.[8,9]

Poly(lactic acid) (PLA) undergoes hydrolytic degradation via the random scission of the ester backbone. It degrades into lactic acid, a normal human metabolic byproduct, which is broken

down into water and carbon dioxide. Because the hydrolytic degradation of aliphatic polyesters is autocatalyzed by carboxylic end groups generated by the chain scission of the ester bonds, solid films degrade faster than porous scaffolds, and the degradation rate of the porous structures increases with increasing pore wall thickness.[10–13] The porosity and pore size thus influence the degradation and release of the degradation products.[14–16]

It has been established that PLA hydrolysis proceeds in three stages.[17,18] During the first stage, the aqueous solution penetrates the polymer, initiating hydrolytic degradation, mainly in the amorphous regions. At this stage, a rapid decrease in the molecular weight is observed but without significant mass loss because the broken molecules are still not soluble in water and remain inside the sample. In the second stage, the mass loss increases, and lactic acid monomer formation is observed with a slight change in molecular weight. At this time, the long polymer chains are converted into shorter water-soluble fragments that dissolve into the medium [PLA becomes soluble in water when it has a number-average molecular weight (M_n) < 20.000 g/mol]. The hydrolysis of soluble oligomers continues in the third stage until the polymer is totally hydrolyzed into monomer lactic acid. PLA is present in two stereopolymer forms: poly(L-lactic acid) (PLLA) and poly(D-lactic acid) (PDLA). The complete degradation of PDLA has been observed *in vivo* between periods of 10 months and 4 years; this depends on its molecular weight, degree of crystallinity, material shape, and implantation site.[19] PLLA is more crystalline and has a lower degradation rate than PDLA.

PLLA has received approval from the U.S. Food and Drug Administration for human clinical use.[20] It exhibits mechanical properties suitable for human tissue engineering applications and has been widely used to guide the regeneration of bone and cartilage.[21–24] Its mechanical properties are affected by degradation from the start of the process. Vieira et al.[25] found that the decrease in the tensile strength of polylactic acid/polycaprolactone (PLA/PCL) fibers followed the same trend as the drop in the molecular weight. Kang et al.[26] observed a linear fall in the compressive strength from 10.5 to 7 MPa in a 6-week degradation of porous PLLA scaffolds in simulated body fluid (SBF). Gaona et al.[27] studied the hydrolytic degradation of PLA/PCL blend membranes showing the mutual influence of the degradation of both phases. Tsuji and coworkers[28,29] studied the hydrolytic degradation of PLLA films in phosphate buffered saline solution as a function of their crystallinity and found that the Young's modulus (E_S) of the PLLA specimens decreased monotonously in the first 8 months. Interconnected porosity and pore size followed by permeability were the important factors affecting the mechanical properties of the scaffold.[30,31] There has been no agreement in the literature on the target mechanical properties of a scaffold for bone tissue engineering.[32] As stated by Rezwan et al.,[33] in general, the scaffold should have sufficient properties to prevent pore collapse during implantation. Human cancellous bone has a compressive strength of 4–12 MPa, a tensile strength of 1–5 MPa, and an elastic modulus of 0.1–0.5 GPa;[32] these properties can serve as guidance for the design of scaffolds. The initial mechanical requirements become less demanding with extended time of implantation because the regenerated tissue in the pores of the scaffold contributes to the mechanical properties and compensates for the loss of scaffold modulus caused by its degradation. There is also no established degradation rate; the recommendation is that the porous structure should keep its integrity during the first weeks after implantation.[32] *In vivo* experiments have demonstrated higher degradation rates than *in vitro* ones.[15]

In a previous article, our group proposed a porous PLLA scaffold with double porosity: micropores generated by dioxane solvent with a freeze-extraction technique and macropores produced by the leaching of macroporogen spheres. A study was carried out on the influence of the preparation parameters on its structure and mechanical properties,[34] and the material was proposed for cartilage[35] and bone regeneration after being coated with a biomimetic apatite layer.[36] In this study, we examined the evolution of the properties of the PLLA scaffold after different degradation times in a phosphate-buffered saline solution. The novelty of this study was that the scaffold preparation method allowed PLLA to crystallize to its maximum capacity. This high crystallinity was reached during the removal of the porogen with ethanol at 37°C and had an important role in the evolution of the scaffold's properties with the degradation time. Although we observed changes in the molecular weight with the time of degradation, no mass loss was recorded, as the chains remain entrapped in the crystalline regions. The high crystallinity of our scaffold also hindered the incorporation of degraded chains in the crystals, as usually has occurred in other lower crystalline scaffolds found in studies in the literature. We emphasize here these novel aspects in the degradation of this highly crystalline PLLA scaffold.

EXPERIMENTAL

Materials

Medical-grade PLLA (PURASORB PL 18), with a viscosity of 1.8 dL/g and a weight-average molecular weight (M_w) of 165,000 g/mol, was purchased from Purac Biomaterials (The Netherlands). Poly(ethyl methacrylate) (PEMA) spheres from Elvacite (Elvacite 2043 acrylic resin), with diameters ranging from 120 to 200 μm, were used as a macroporogen, and 1,4-dioxane (98% pure) from Sigma Aldrich was used as a PLLA solvent and microporogen. Ethanol (99% pure) from Scharlab was used as a low-temperature solvent for dioxane.

Preparation of the PLLA Scaffold

The PLLA scaffold was prepared by a combination of the freeze-extraction and porogen-leaching methods.[37,38] A solution of PLLA in 1,4-dioxane with 15 wt % PLLA was homogeneously mixed at room temperature with the PEMA spheres in mass proportion of 1:1 w/w in a Teflon mold and immediately frozen with liquid nitrogen. Cold ethanol at −20°C was then poured on the frozen sample to dissolve the crystallized dioxane. Dioxane extraction was conducted in a cold ethanol bath (−20°C), in which the ethanol was renewed at least four times. Then, the extraction of the PEMA porogen was carried out with ethanol at 40°C under slow stirring. The ethanol was changed until no PEMA deposit was left on a glass when a drop of the extraction liquid was evaporated. After extraction, the scaffold was dried in an air atmosphere for 24 h and then *in vacuo* to a constant weight, first at room temperature and later at 40°C. Cylinders

6 mm in diameter and 4 mm in height were punched from larger pieces of the scaffold.

Degradation Experiments

Each sample of known mass was immersed in 2 mL of PBS at 37°C and maintained for 3, 4.5, 6, and 12 months under static conditions. The PBS bath was renewed every 2 weeks. After different immersion times in PBS, three replicates were washed several times with distilled water with gentle shaking, then dried (as described previously), and weighed. The mass loss of the different scaffolds with the time of degradation was evaluated with the following equation:

$$\text{Mass loss}\,(\%) = \frac{m_i - m_f}{m_i} \times 100 \quad (1)$$

where m_i is the initial mass and m_f is the final mass of the sample. A balance (Mettler-Toledo) with a sensitivity of 0.01 mg was used to weigh the samples, which were then analyzed by different methods to determine the influence of the degradation time on the scaffold properties.

Scanning Electron Microscopy (SEM)

The morphology of the samples was analyzed with a JEOL JSM 6300 scanning electron microscope at an accelerating voltage of 15 kV. The samples were mounted onto copper holders and gold-sputtered for observation. Scaffold sections were excised with a razor blade to observe both the surface and cross section.

Microtomography (μCT)

μCT was carried out to define the average macropore size. The image files (Digital Imaging and Communication in Medicine) provided by μCT were the main input for building the geometric model of the scaffold. Images of the whole sample were obtained by 360° rotational scanning. A GE Healthcare eXplore Locus SP μCT was used with an X-ray filter number 2, a 45-kV voltage, and 120 mA of power. The resolution of the equipment was 8 μm. Ninety Digital Imaging and Communication in Medicine files were obtained for each sample (one image for each 4.0° rotation). Five replicates for each degradation time (0, 3, 4.5, and 6 months) were measured to determine the corresponding macropore size.[37,39]

Mechanical Properties Under Compression

The mechanical properties of the degraded scaffolds were measured under wet conditions in two static uniaxial tests: unconfined compression (UC) and confined compression (CC).[34] During the UC test, the scaffold could generate a lateral deformation when a load or displacement was applied. In the CC test, the lateral deformation of the scaffold was constrained because the sample was in a confined space. Mollica et al.[40] described the development of a typical stress–strain curve for scaffolds submitted to uniaxial compression tests. After the first small region in which the struts and plates were compressed, once a critical load was reached, they buckled, giving way to a plateau region, in which the apparent density of the material grew until the stress–strain curve increased again (third region) until the failure or total collapse of the structure occurred.[40] For the UC and CC tests, either the apparent E_S or the aggregate modulus (H_A) value was calculated, respectively, from the slope of the first linear region of the stress–strain curve and with the initial cross-sectional area.[34] Additionally, the yield strength was determined between the first and second region. For this study, the first point after the linear region at the stress–strain curve was determined as the lower yield limit (Y_L), at which plastic deformation began to occur.[41,42]

Before we carried out the wet compression tests, the samples were maintained in PBS solution for 24 h at a temperature of 37°C.[40] The tests began with a predeformation of 4% of the total thickness of the sample at 0.001 mm/s to eliminate the nonlinearity generated by the geometrical variability of the samples and to normalize an initial reference test point.[34,43] A monotonic ramp performed at a 0.01 mm/s crosshead velocity was carried out with an Instron MicroTester 5548 with a precision of 0.0001 N, a force and displacement of 0.001 mm, and a 50-N load cell.[34] The dimensions of the sample were measured before and after the test. Five replicates for each degradation time and UC and CC test were measured to determine the corresponding E_S and H_A modulus and the Y_L limit. Finally, Poisson's ratio (ν) described the lateral expansion during axial compression and was defined as the ratio between the lateral and axial strains. For each degradation period, ν was deduced from the E_S and H_A averaged data with the theory proposed in refs. 44–46 and according to the following equation:

$$E_s = \frac{(1+\nu)(1-2\nu)}{1-\nu} H_A \quad (2)$$

Permeability

The permeability was measured by the quantification of the ability of a porous medium to conduct fluid flow through its interconnected pores when subjected to pressure,[47,48] regardless of the fluid used in the measurement and the thickness of the porous sample.[49,50]

The permeability test was developed under conditions for which Darcy's law [eq. (3a)] was valid, that is, for Reynolds numbers lower than 8.6:[34,47–51]

$$k = \frac{\mu t}{A}\frac{Q}{\Delta p} \quad (3a)$$

$$\Delta p = \Delta p_{\text{scaffold}} - \Delta p_{\text{chamber}} \quad (3b)$$

where k is the intrinsic permeability (m^2), μ is the dynamic fluid viscosity (deionized water $\mu = 10^{-3}$ Pa s), t is the specimen thickness, A is the cross-sectional area, Q is the volumetric flow rate, and Δp is the total pressure drop across the scaffold sample (Pa). The total pressure drop measured with the scaffold specimen inside the chamber is $\Delta p_{\text{scaffold}}$, whereas $\Delta p_{\text{chamber}}$ is the measurement for the empty chamber [eq. (3b)].[52] Because of the test configuration, the measured pressure drop was attributed to the scaffold microstructure and the section change. $\Delta p_{\text{scaffold}}$ and $\Delta p_{\text{chamber}}$ were measured between two points of the permeameter chamber with a pressure meter (Testo 510, with a precision of $\pm$ 0.1% and an operating range of 0–2000 hPa). Five samples comprising cylinders 6 mm in diameter and 3.02 ± 0.02 mm in thickness were tested for each degradation period. In accordance with the experimental protocol, the fluid flow through the scaffold was varied by the control of the flow

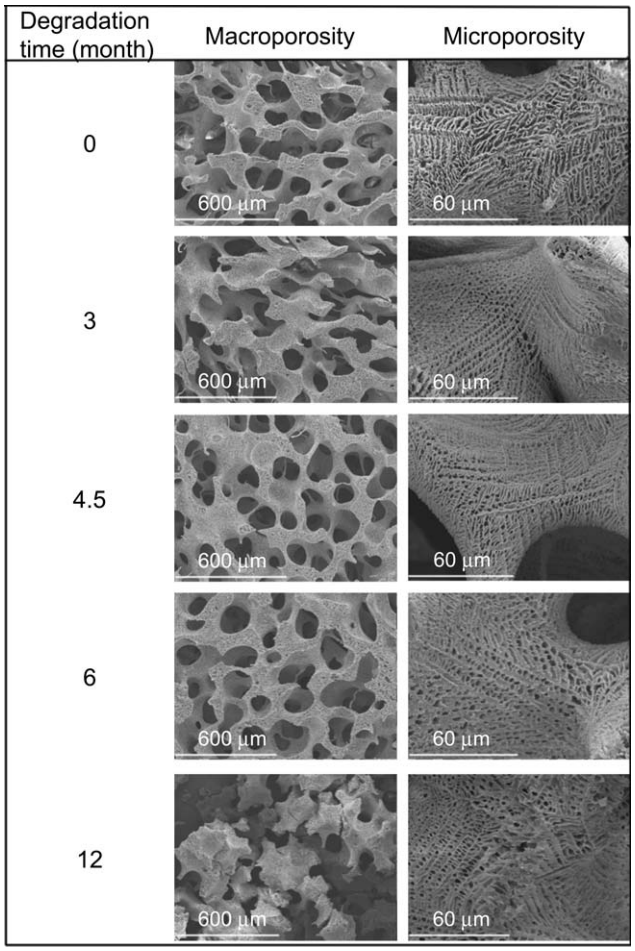

Figure 1. SEM pictures of a section of a PLLA scaffold showing the effects of static degradation in PBS on the scaffold morphology at different magnifications and for different degradation times.

rate (20, 40, and 60 mL/min).[34] The $\Delta p_{scaffold}$ generated in each case was measured and then averaged out to determine the permeability of the structure with eq. (3a).

Differential Scanning Calorimetry (DSC)

The thermal properties of the scaffolds were determined by a Pyris 1 calorimeter (PerkinElmer). Dry nitrogen gas was passed through the DSC cell at a flow rate of 20 mL/min. The temperature of the equipment was calibrated with the melting points of indium and zinc. The heat of fusion of indium was used to calibrate the heat flow. Each sample underwent two heating processes from 0 to 210°C at a rate of 10°C/min. The samples were cooled between scans from 210 to 0°C at a rate of −10°C/min. The data from all three scans were collected for subsequent analysis. The first scan measured the effect of the previous history of the material (in our case, the scaffold preparation followed by the degradation processes). As all of the samples were melted and crystallized under the same conditions, the second heating scan depended on the material properties.[53] The crystallinity (x_c) was assumed to be proportional to the experimental heat of fusion according to the following equation:

$$x_c(\%) = \frac{\Delta h_m}{\Delta h_m^0} \times 100 \quad (4)$$

where Δh_m is the measured enthalpy of fusion of the sample and $\Delta h_m^0 = 93.1$ J/g is the enthalpy of fusion of the completely crystalline material (i.e., that corresponding to a crystal of infinite thickness).[54,55]

Gel Permeation Chromatography (GPC)

The M_w values of the samples were determined with a gel permeation chromatograph at 30°C with a Waters Breeze GPC system with a 1525 binary High-performance liquid chromatography (HPLC) pump (Waters Corp., Milford, MA) equipped with a 2414 refractive-index detector and Waters Styragel HR tetrahydrofuran columns. Tetrahydrofuran was used as the eluent at a flow rate of 0.5 mL/min. The calibration curve was prepared with monodisperse polystyrene standards from Shodex (Showa Denko K.K., Kawasaki, Japan).

Thermogravimetric Analysis (TGA)

TGA (SDTQ600 thermogravimetric analyzer from TA Instruments) was performed to evaluate the effect of the static degradation in PBS on the thermal stability of the scaffolds. The samples were subjected to a temperature ramp from room temperature up to 800°C at 20°C/min under nitrogen flow (50 mL/min).

Statistical Analysis

For the experimental data (E_S, H_A, Y_L, and k), a normal distribution was tested by the Anderson–Darling test. A one-way analysis of variance was performed for parametric comparison. The statistical significance was set at a mean of $p < 0.05$ with a 95% confidence interval.[46] The statistical methods applied were calculated with Minitab software. Finally, the results are presented as the mean plus or minus the standard deviation.

RESULTS

Morphology of the Scaffolds

As shown in the SEM micrographs of the samples sections in Figure 1, the macrostructures and microstructures of the different scaffolds submitted to different periods of degradation did not present significant changes for a period of up to 6 months. The trabeculae seemed to be intact, and the macropores appeared to maintain their size and interconnectivity. However, a significant change was observed after 1 year, when most of the trabeculae were observed to be broken in the SEM pictures. In fact, at this time, they disaggregated easily when they were manipulated. No changes in the micropore dimensions were observed for any degradation time, even after 1 year of incubation in PBS. No morphological differences were observed between the section and surface of the scaffolds.

Mass Evolution

The mass loss as a function of the degradation time was determined with eq. (1). There were no significant changes in the samples mass for the first 6 months of degradation in PBS, and only a 2% mass loss was measured after 1 year.

Mechanical Properties

The influence of the static degradation experiment on the mechanical properties of the PLLA scaffold was evaluated by a compression test (UC and CC), from which the elastic modulus was calculated (see the representative stress vs strain curves for

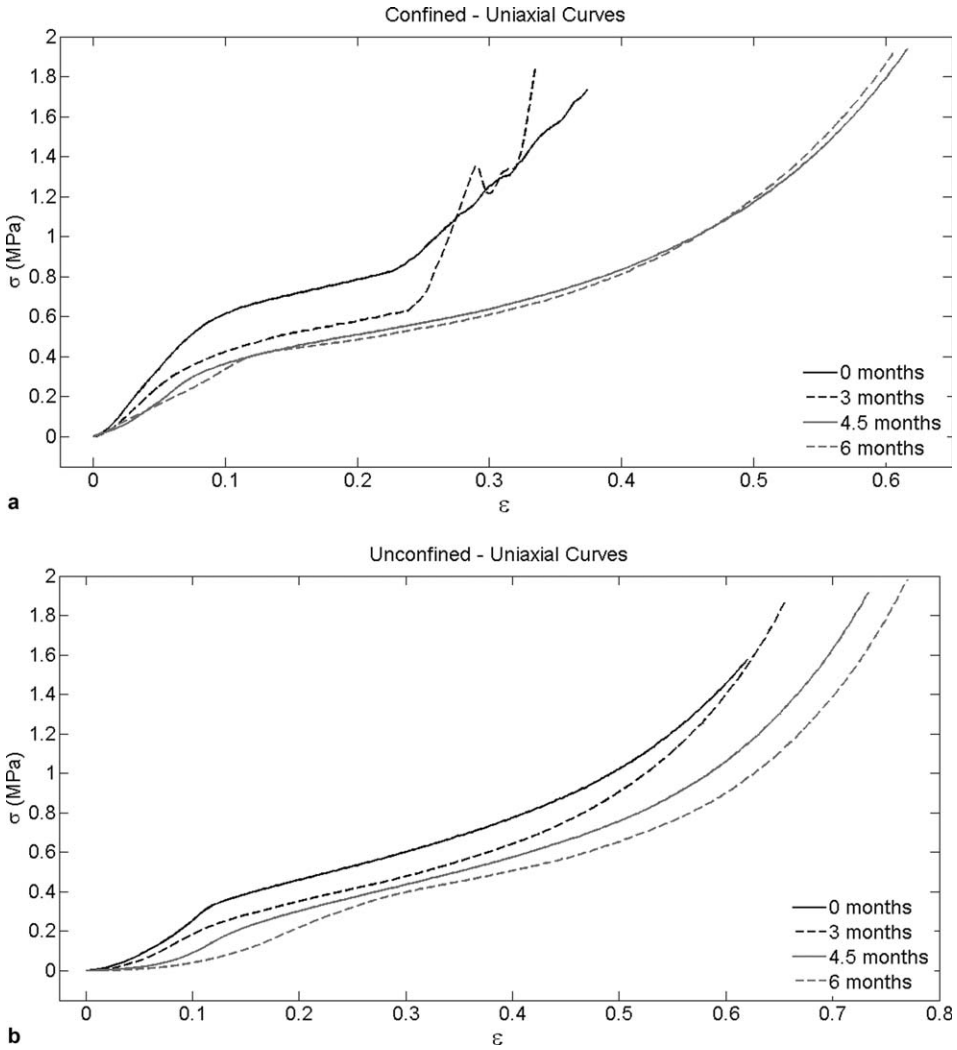

Figure 2. Stress (σ)–strain (ε) curves of the CC and UC uniaxial compression tests after 0, 3, 4.5, and 6 months of static degradation of PLLA scaffolds.

each time of degradation in Figure 2 and the calculated mean parameters in Table I).

The apparent E_S and H_A values decreased with the degradation time. E_S was reduced by 27.16% between the initial and final immersion periods [from $E_S = 3.43 \pm 0.25$ MPa at 0 days of degradation to $E_S = 2.50 \pm 0.30$ MPa after 6 months of degradation]. H_A was reduced by 44.27% [from $H_A = 7.73 \pm 0.67$ MPa at 0 days of degradation to $H_A = 4.31 \pm 0.96$ MPa after 6 months of degradation]. The v factor was also seen to decrease with the degradation time (Table I).

For the UC test, the strain required to achieve the lower Y_L was higher than that reported for the CC test (Table I), and it was observed to decrease with the degradation time (11.08% after 6 months of degradation). This trend was opposite to that of the strain data reported for the CC tests, in which the deformation increased by 97.5% in the same period of time. However, in both cases (UC and CC), after 6 months of degradation, and with consideration of the experimental dispersion, the plastic zone started at the same strain level. Significant differences were found in the CC results between the 6 months of degradation and the non-degraded or 3 months degradation periods ($p < 0.05$). In the UC test, the obtained stress level for Y_L decreased between 0 and 3 months of degradation, whereas the CC data showed the opposite trend. After the 3 months degradation period, the Y_L stress results showed a change of tendency in both the UC and CC tests (Table I).

Permeability

The results of the permeability test are shown in Table I. The k value of the scaffold structure increased with the immersion time. After 6 months of degradation, the permeability rose by 165.23% [from 1.20×10^{-10} to 3.18×10^{-10} m^2]; this was accompanied by an increase in the experimental dispersion. The results at $t = 6$ months showed the highest dispersion with a value of $\pm 5.79 \times 10^{-11}$ m^2 (Table I). The statistical treatment determined significant differences ($p < 0.05$) for the k values between the initial condition and the 4.5 and 6 months degradation periods with no significant differences between them.

Calorimetric Properties

The influence of the static degradation process on the calorimetric properties of the PLLA scaffold was evaluated by DSC

Table I. Evolution of the Macropore Size, Permeability, Apparent E_S Values for the UC Test, and H_A Values for the CC Test as a Function of the Degradation Time for the PLLA Scaffolds Under Static Conditions

Degradation time (months)	Macropore size (μm)	UC test			CC test				
		E_S (MPa)	Stress Y_L (MPa)	Strain Y_L	H_A (MPa)	Stress Y_L (MPa)	Strain Y_L	ν	k (m^2)
0	127 ± 5	3.43 ± 0.25	0.38 ± 0.08	0.17 ± 0.02	7.73 ± 0.67	0.34 ± 0.06	0.05 ± 0.01	0.41	$1.20 \times 10^{-10} \pm 7.71 \times 10^{-12}$
3	184 ± 10	3.06 ± 0.12	0.41 ± 0.07	0.16 ± 0.02	5.46 ± 0.95	0.24 ± 0.04	0.05 ± 0.01	0.37	$1.77 \times 10^{-10} \pm 2.96 \times 10^{-11}$
4.5	206 ± 2	2.94 ± 0.33	0.30 ± 0.09	0.15 ± 0.02	4.56 ± 0.84	0.35 ± 0.09	0.06 ± 0.01	0.34	$2.97 \times 10^{-10} \pm 3.74 \times 10^{-11}$
6	232 ± 8	2.5 ± 0.30	0.23 ± 0.03	0.15 ± 0.03	4.31 ± 0.96	0.34 ± 0.05	0.10 ± 0.02	0.36	$3.18 \times 10^{-10} \pm 5.79 \times 10^{-11}$

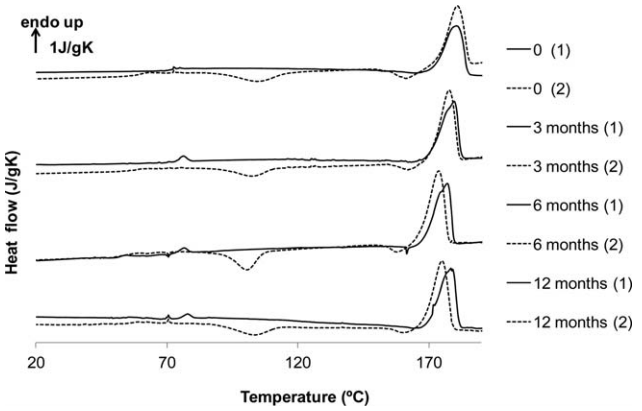

Figure 3. Normalized heat flow of the (1) first and (2) second DSC heating scans after 0, 3, 6, and 12 months of static degradation of the PLLA scaffolds. The heat flow was normalized by the mass of the sample and the heating rate (10°C/min). The arrow represents a unit of heat flow (J/g K).

scans. The crystallinity after the first heating scan was representative of the thermal history of the sample (porous scaffold fabrication and degradation), whereas that taken from the second heating scan (2) was representative of the properties of the previously degraded and melted bulk sample. The degraded scaffolds presented a double melting peak in the first scan (Figure 3). The second heating scan showed differences with the first one; two crystallization peaks appeared, cold crystallization took place around 100°C, but a smaller exotherm appeared at higher temperatures, with a minimum of around 160°C. The second crystallization peak was characteristic of PLLA samples crystallized at low temperatures (as was the case for the crystals formed during heating at temperatures immediately above the glass transition), and this was explained by the recrystallization process.[56] The double melting peak did not appear in the second heating scan, whereas the maximum of the melting peak appeared at a lower temperature in the second heating scan. This could have been due to a decrease in the molecular weight, which produced thinner, less perfect lamellae.[57]

The enthalpic glass-transition temperature (T_g; determined as the intersection temperature of the enthalpy lines at the liquid and glassy states in the enthalpy vs temperature diagram) was calculated from these curves (Table II). The crystallinity values after the first and second heating scans are presented in Table II as well. They were calculated by the integration of the heat flow trace with respect to a baseline joining a point

Table II. Crystallinity, x_c and Glass Transition Temperature, T_g After the (1) First (x_{c1} and T_{g1}, respectively) and (2) Second (x_{c2} and T_{g2}, respectively) DSC Scans of the Scaffolds After Different Static Degradation Times in PBS at 37°C

	x_c (%)		T_g (°C)	
Degradation time (months)	x_{c1}	x_{c2}	T_{g1}	T_{g2}
0	48	13	72	58
3	46	22	72	58
6	51	27	73	54
12	49	38	75	54

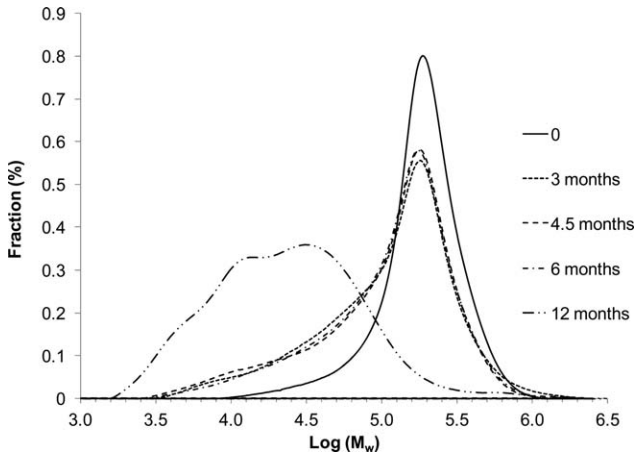

Figure 4. GPC curves representing the fraction (percentage) of chains as a function of log M_w for the PLLA scaffolds after 0, 3, 4.5, 6, and 12 months of hydrolytic degradation.

immediately above the glass transition and one after the melting. This way, the crystallinity values obtained after the second scan corresponded to the crystallinity obtained in the cooling scan, after the first melting. An endothermic peak appeared in all of the degraded samples and on the glass-transition process, but it did not appear in the nondegraded ones. This peak was associated with the physical aging suffered by the amorphous phase of the semicrystalline samples annealed for quite long times at 37°C; it was around 30° below its glass transition. This peak disappeared in the second scan because the samples were heated immediately after they were cooled from high temperatures. The small value of the heat-capacity increment at the glass transition (Δc_p) in the first scan was due to the high crystallinity of the sample. The scaffold glass-transition temperature (T_{g2}) and scaffold crystallinity (x_{c2}) at the second heating were smaller than those in the first one for all of the degradation times, and consequently, Δc_p at T_g was higher in the second scan than in the first one. T_g at day 0 shifted from 72°C in the first scan to 58°C in the second. The crystallinity and glass-transition values in the first heating scan after different degradation times remained almost constant. In the second scan, the crystallinity increased with the degradation time from 13% in the nondegraded sample up to 38% after 1 year of degradation.

GPC

From the molecular weight distribution functions obtained by GPC (Figure 4), we were able to analyze the effect of the degradation time on the M_w and PLLA polydispersity index (M_w/M_n; the results are shown in Table III). The nondegraded PLLA scaffold presented a narrow molecular weight distribution function, with its maximum around 2×10^5 g/mol. A higher fraction of short chains was generated with the degradation time, and the weight average molar mass decreased. The polydispersity index rose as the GPC curves broadened to lower molecular masses.

Table III. M_w and Polydispersity Index (M_w/M_n) Values After Different Hydrolytic Degradation Times in PBS at 37°C

Degradation time (months)	M_w (kDa)	M_w/M_n
0	165.4	1.4
3	126.4	2.3
4.5	125.2	2.4
6	127.6	2.2
12	34.4	2.7

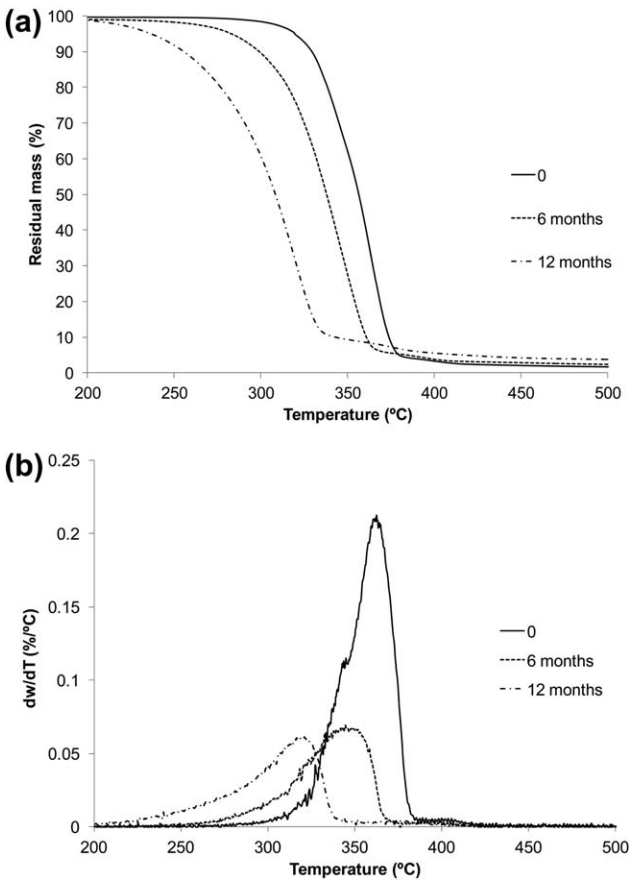

Figure 5. (a) Residual mass as a function of temperature for the PLLA scaffolds after 0, 6, and 12 months of hydrolytic degradation and (b) dw/dT as a function of temperature for the same samples and conditions.

TGA

The PLLA scaffolds were thermally degraded to evaluate the effect of the hydrolytic degradation in PBS on the thermal stability of the polymer chains. The TGA curves shown in Figure 5(a) represent the residual mass of the thermally degraded scaffolds. The first derivative of mass as a function of the temperature (dw/dT) is also shown in Figure 5(b). The derivative curve for the nondegraded PLLA indicated that PLLA decomposition took place in only one step, as it presented only one peak. The maximum peak temperature gradually decreased with the degradation time; it was 360°C for the nondegraded scaffold and 315°C after 1 year of degradation. The nondegraded scaffold started to thermally degrade around 300°C, whereas the product hydrolytically degraded for 1 year started this process around 210°C [Figure 5(a)].

DISCUSSION

The degradation of the polymer chains could be detected by GPC analysis from the first 3 months (Figure 4). Although the

SEM microphotographs do not clearly show that degradation started on the pore surface (Figure 1), the μCT images show that macropore dimensions increased with time (Table I), which was consistent with the rise in the permeability. The GPC curves show that a major fraction of the chains kept their molecular weight, as the principal peak of the degraded samples did not change its position but did fall in intensity (Figure 4). This evolution, together with the increased macropore dimensions and permeability, is characteristic of polymers with surface degradation and was related to the PLLA hydrophobicity. The PLLA hydrolysis produced carboxylic end groups that favored water penetration into the bulk material. After 1 year, the GPC curve shifted toward a lower molecular weight as the entire volume of the material became affected by the degradation process. The evolution of the molecular weight with degradation time was consistent with previous results obtained by Tsuji et al.[28] for crystallized PLLA. The weight loss, however, was the least notable effect in the degradation test; this suggested that the degraded chains remained entrapped in the material, protected by the crystalline regions. The low degradation rate, together with the increasing permeability, makes this scaffold suitable for bone regeneration. In our previous work on animal implantation,[36] the scaffold maintained its mechanical integrity and stability and allowed new tissue formation after 6 weeks of implantation in the subchondral bone of sheep.

Degradation affected the scaffold's mechanical properties. As shown in Table I, E_S, like the Poisson's rate, decreased with the degradation time (by 27 and 15% after 6 months, respectively), after which the porous structure lost its biaxial deformation capacity. Moreover, the samples reach the plasticization limit at lower deformation levels because the lower Y_L decreased with the degradation time.

H_A also decreased with the degradation time (44% after 6 months). The difference between E_S and H_A decreased with the degradation time, and consequently, v decreased with the degradation time. The transition to the plastic region, measured through Y_L in the confined test, remained approximately constant for the 3 first months of degradation. However, between 4.5 and 6 months, this zone moved toward higher deformation levels. In many applications, for example, in articular cartilage replacement, the scaffold works in a confined space so that the confined results are more important than those of the UC test.

The freeze-extraction process generated highly crystallized scaffolds (50%; Table I) without the ability to crystallize further during the first heating scan, so no cold crystallization peak was observed. No significant change in the crystallinity with the degradation time was observed in the first heating scan. This was because the degraded chains, which usually belong to the amorphous regions, remained immobile, trapped between the crystalline regions. However, the crystallinity increased in the second heating scan. After melting, the shorter chains produced by degradation, had a higher mobility and could reorganize into crystallites. The second heating scan showed the degradation effect through increased crystallinity. Degradation had no significant effect on the scaffold T_g; this was consistent with the results obtained by Tsuji et al.[28] on the hydrolytic degradation of PLLA in PBS. Previous degradation studies on PLLA porous samples with lower initial crystallinities[15] found higher degradation rates (30% weight loss after 40 weeks) and an increase in the crystallinity with the degradation time.

The scission of the polymer chains measured by GPC also influenced the thermal stability of the samples [Figure 5(a)]. Persenaire et al.[58] described the influence of the molecular weight on PCL thermal degradation. In the case of PLLA, the shift observed in the temperature of the derivative peak could have been a consequence of two phenomena. First, the higher proportions of carboxyl and hydroxyl groups in the degraded samples could have acted as catalyzers in the scission of ester bonds. Second, because the degraded samples had shorter chains, the diffusion of volatile species should have been easier, and the onset of mass loss should have been produced at lower temperatures.

The evolution of the properties presented in this article suggests that the polymer was in its first stage of degradation, at least during the 12 months of this experiment. There were signs of transition toward the second degradation stage around 12 months, as indicated by the morphological and mass changes.

CONCLUSIONS

The freeze-extraction fabrication process led to highly crystalline scaffolds that were able to maintain their morphology after 6 months of static degradation. The macroporosity seemed to be affected by degradation, but no change in the microporosity was observed. Although the morphological changes in the form of the surface erosion were quite slight, when the samples were tested in the permeameter, the more degraded samples suffered higher surface erosion, and consequently, the permeability increased considerably with degradation time. The scaffolds' high molecular weight and crystallinity made them highly resistant to degradation, and no changes in the mass or crystallinity measured in the first scan were observed after 1 year of degradation. Although degradation attacked the amorphous phase, the degraded chains were trapped in the samples between the crystalline regions. Degradation produced shorter chains with higher mobilities; this produced the increased crystallinity observed in the second heating scan and a decrease in the scaffold thermal stability during degradation. The hydrolytic degradation of PLLA affected its mechanical properties, as the main parameters (E_S, H_A, v, and Y_L) decreased with the degradation time.

ACKNOWLEDGMENTS

The authors acknowledge the support of the Instituto de Salud Carlos III, Ministerio de Economía y Competitividad, and the European Commission through FP7-ERANet EuroNanoMed 2011 PI11/03032 and FP7-PEOPLE-2012-IAPP (contract grant number PIAP-GA-2012–324386). The Biomedical Research Networking Center in Bioengineering, Biomaterials, and Nanomedicine is an initiative funded by the VI National R&D&i Plan 2008–2011, Iniciativa Ingenio 2010, and Consolider Program. Biomedical Research Networking Center actions are financed by the Instituto de Salud Carlos III with assistance from the European Regional Development Fund. The authors also thank the Tissue Characterization Platform of the Biomedical Research Networking Center in

Bioengineering, Biomaterials, and Nanomedicine for its technical support. They also thank the Linguistic Assistance Services of the Language Centre, Universitat Politecnica de Valencia, for their help in revising this article.

REFERENCES

1. Zhao, J.; Yuan, X.; Cui, Y.; Ge, Q.; Yao, K. *J. Appl. Polym. Sci.* **2004**, *91*, 1676.
2. Hutmacher, D. *J. Biomater. Sci. Polym. Ed.* **2001**, *12*, 107.
3. Butler, D.; Goldstein, S.; Guilak, F. *J. Biomech. Eng. Trans. ASME* **2000**, *122*, 570.
4. Budyanto, L.; Goh, Y. Q.; Ooi, C. P. *J. Mater. Sci. Mater. Med.* **2009**, *20*, 105.
5. Woodruff, M. A.; Lange, C.; Reichert, J.; Berner, A.; Chen, F.; Fratzl, P.; Schantz, J.; Hutmacher, D. W. *Mater. Today* **2012**, *15*, 430.
6. Hollister, S. *Nat. Mater.* **2005**, *4*, 518.
7. Hutmacher, D. *Biomaterials* **2000**, *21*, 2529.
8. Chiquet, M.; Reneda, A.; Huber, F.; Fluck, M. *Matrix Biol.* **2003**, *22*, 73.
9. Diego, R. B.; Estelles, J. M.; Sanz, J. A.; Garcia-Aznar, J. M.; Sanchez, M. S. *J. Biomed. Mater. Res. B* **2007**, *81*, 448.
10. Pitt, C.; Chasalow, F.; Hibionada, Y.; Klimas, D.; Schindler, A. *J. Appl. Polym. Sci.* **1981**, *26*, 3779.
11. Lu, L.; Peter, S.; Lyman, M.; Lai, H.; Leite, S.; Tamada, J.; Vacanti, J.; Langer, R.; Mikos, A. *Biomaterials* **2000**, *21*, 1595.
12. Lu, L.; Peter, S.; Lyman, M.; Lai, H.; Leite, S.; Tamada, J.; Uyama, S.; Vacanti, J.; Langer, R.; Mikos, A. *Biomaterials* **2000**, *21*, 1837.
13. Li, S.; Garreau, H.; Vert, M. *J. Mater. Sci.: Mater. Med.* **1990**, *1*, 123.
14. Odelius, K.; Hoglund, A.; Kumar, S.; Hakkarainen, M.; Ghosh, A. K.; Bhatnagar, N.; Albertsson, A. *Biomacromolecules* **2011**, *12*, 1250.
15. Gong, Y.; Zhou, Q.; Gao, C.; Shen, J. *Acta Biomater.* **2007**, *3*, 531.
16. Zhao, J.; Han, W.; Tu, M.; Huan, S.; Zeng, R.; Wu, H.; Cha, Z.; Zhou, C. *Mater. Sci. Eng. C* **2012**, *32*, 1496.
17. Hakkarainen, M.; Albertsson, A.; Karlsson, S. *Polym. Degrad. Stab.* **1996**, *52*, 283.
18. Zhang, X.; Espiritu, M.; Bilyk, A.; Kurniawan, L. *Polym. Degrad. Stab.* **2008**, *93*, 1964.
19. Chen, J.; Chu, B.; Hsiao, B. S. *Biomaterials* **2003**, *24*, 1167.
20. Thomson, R.; Wake, M.; Yaszemski, M.; Mikos, A. *Biopolymers II* **1995**, *122*, 245.
21. Lee, H.; Jin, G.; Shin, U. S.; Kim, J.; Kim, H. *J. Mater. Sci.: Mater. Med.* **2012**, *23*, 1271.
22. Li, W.; Tuan, R. *Macromol. Symp.* **2005**, *227*, 65.
23. Ma, J.; He, X.; Jabbari, E. *Ann. Biomed. Eng.* **2011**, *39*, 14.
24. Dai, L.; Li, D.; He, J. *J. Appl. Polym. Sci.* **2013**, *130*, 2257.
25. Vieira, A. C.; Vieira, J. C.; Ferra, J. M.; Magalhaes, F. D.; Guedes, R. M.; Marques, A. T. *J. Mech. Behav. Biomed. Mater.* **2011**, *4*, 451.
26. Kang, Y.; Yin, G.; Luo, L.; Wang, K.; Zhang, Y. *Adv. Biomater. VII* **2007**, *342*, 273.
27. Gaona, L. A.; Gómez Ribelles, J. L.; Perilla, J. E.; Lebourg, M. *Polym. Degrad. Stab.* **2012**, *97*, 1621.
28. Tsuji, H.; Mizuno, A.; Ikada, Y. *J. Appl. Polym. Sci.* **2000**, *77*, 1452.
29. Tsuji, H.; Ikada, Y. *Polym. Degrad. Stab.* **2000**, *67*, 179.
30. Freyman, T. M.; Yannas, I. V.; Gibson, L. *J. Prog. Mater. Sci.* **2001**, *46*, 273.
31. Li, S. H.; de Wijn, J. R.; Li, J. P.; Layrolle, P.; de Groot, K. *Tissue Eng.* **2003**, *9*, 535.
32. Wagoner Johnson, A. J.; Herschler, B. A. *Acta Biomater.* **2011**, *7*, 16.
33. Rezwan, K.; Chen, Q.; Blaker, J.; Boccaccini, A. *Biomaterials* **2006**, *27*, 3413.
34. Acosta-Santamaría, V.; Deplaine, H.; Mariggió, D.; Villanueva-Molines, A. R.; García-Aznar, J. M.; Gómez Ribelles, J. L.; Doblaré, M.; Gallego Ferrer, G.; Ochoa, I. *J. Non-Cryst. Solids* **2012**, *358*, 3141.
35. Izal, I.; Aranda, P.; Ripalda, P.; Sanz-Ramos, P.; Mora, G.; Granero-Moltó, F.; Deplaine, H.; Gómez Ribelles, J. L.; Gallego Ferrer, G.; Acosta, V.; Ochoa, I.; García-Aznar, J. M.; Andreu, E. J.; Monleón-Pradas, M.; Doblaré, M.; Prósper, F. *Knee Surg. Sports Traumatol. Arthrosc.* **2013**, *21*, 1737.
36. Deplaine, H.; Lebourg, M.; Ripalda, P.; Vidaurre, A.; Sanz-Ramos, P.; Mora, G.; Prósper, F.; Ochoa, I.; Doblaré, M.; Gómez Ribelles, J. L.; Izal-Azcárate, I.; Gallego Ferrer, G. *J. Biomed. Mater. Res. B* **2013**, *101*, 173.
37. Lebourg, M.; Suay Anton, J.; Gomez Ribelles, J. L. *J. Mater. Sci.: Mater. Med.* **2010**, *21*, 33.
38. Ho, M.; Kuo, P.; Hsieh, H.; Hsien, T.; Hou, L.; Lai, J.; Wang, D. *Biomaterials* **2004**, *25*, 129.
39. Alberich-Bayarri, A.; Moratal, D.; Escobar Ivirico, J. L.; Rodriguez Hernandez, J. C.; Valles-Lluch, A.; Marti-Bonmati, L.; Mas-Estelles, J.; Mano, J. F.; Monleon Pradas, M.; Gomez Ribelles, J. L.; Salmeron-Sanchez, M. *J. Biomed. Mater. Res. B* **2009**, *91*, 191.
40. Mollica, F.; Ventre, M.; Sarracino, F.; Ambrosio, L.; Nicolais, L. *Comput. Math. Appl.* **2007**; *53*, 209.
41. Charles, H. T. *Ann. N Y Acad. Sci.* **2006**, *1068*, 429.
42. Harley, B. A.; Leung, J. H.; Silva, E. C. C. M.; Gibson, L. *J. Acta Biomater.* **2007**, *3*, 463.
43. Mark, R.; DiSilvestro, J. *J. Biomech.* **2001**, *34*, 519.
44. Jurvelin, J. S.; Buschmannf, M. D.; Hunziker, E. B. *J. Biomech.* **1997**, *30*, 235.
45. Korhonen, R.; Laasanen, M.; Toyras, J.; Rieppo, J.; Hirvonen, J.; Helminen, H.; Jurvelin, J. *J. Biomech.* **2002**, *35*, 903.
46. Acosta-Santamaría, V. A.; García-Aznar, J. M.; Ochoa, I.; Doblare, M. *Exp. Mech.* **2013**, *53*, 911.
47. Ochoa, I.; Sanz-Herrera, J. A.; Garcia-Aznar, J. M.; Doblare, M.; Yunos, D. M.; Boccaccini, A. R. *J. Biomech.* **2009**, *42*, 257.
48. Chor, M. V.; Li, W. *Meas. Sci. Technol.* **2007**, *18*, 208.
49. Al-Munajjed, A. A.; Hien, M.; Kujat, R.; Gleeson, J. P.; Hammer, J. *J. Mater. Sci. Mater. Med.* **2008**, *19*, 2859.

50. O'Brien, F. J.; Harley, B. A.; Waller, M. A.; Yannas, I.; Gibson, L. J.; Prendergast, P. *Technol. Health Care* **2007**, *15*, 3.

51. Sanz, J. A.; Kasper, C.; van Griensven, M.; Garcia-Aznar, J. M.; Ochoa, I.; Doblare, M. *J. Biomed. Mater. Res. B* **2008**, *87*, 42.

52. Truscello, S.; Kerckhofs, G.; Van Bael, S.; Pyka, G.; Schrooten, J.; van Oosterwyck, H. *Acta Biomater.* **2012**, *8*, 1648.

53. Castilla-Cortazar, I.; Mas-Estelles, J.; Meseguer-Duenas, J. M.; Escobar Ivirico, J. L.; Mari, B.; Vidaurre, A. *Polym. Degrad. Stab.* **2012**, *97*, 1241.

54. Tsuji, H.; Ikada, Y. *Polymer* **1996**, *37*, 595.

55. Lebourg, M.; Suay Anton, J.; Gomez Ribelles, J. L. *Eur. Polym. J.* **2008**, *44*, 2207.

56. Hernández Sánchez, F.; Molina Mateo, J.; Romero Colomer, F.; Salmerón Sánchez, M.; Gómez Ribelles, J. L.; Mano, J. F. *Biomacromolecules* **2005**, *6*, 3291.

57. Hoglund, A.; Odelius, K.; Hakkarainen, M.; Albertsson, A. *Biomacromolecules* **2007**, *8*, 2025.

58. Persenaire, O.; Alexandre, M.; Degee, P.; Dubois, P. *Biomacromolecules* **2001**, *2*, 288.